ce/papers Proceedings in civil engineering

Ernst & Sohn A Wiley Brand

ORIGINAL ARTICLE

ibausil F. A. Finger-Institut für Baustoffkunde Bauhaus-Universität Weimar

Thermodynamic Modeling of Sulfuric and Acetic Acid Attack on Hardened Cement Paste: Effect of Silica Fume

Felix Berger[1] | Neven Ukrainczyk[1] | Andreas Bogner[2] | Astrid Hirsch[2] | Frank Dehn[2] | Eduardus Koenders[1]

Correspondence

Dr. Neven Ukrainczyk
Institute of Construction and Building Materials, Technical University of Darmstadt
Franziska-Braun-Straße 3
64287 Darmstadt, Germany
Email: ukrainczyk@wib.tu-darmstadt.de

[1] Institute of Construction and Building Materials, Technical University of Darmstadt, 64287 Darmstadt, Germany
[2] Institute of Concrete Structures and Buildings Materials, Department Building Materials and Concrete Construction, Karlsruhe Institute of Technology (KIT), 76131 Karlsruhe, Germany

Abstract

The exposure of concrete structures to acid attack is a growing concern. This study employs thermodynamic modeling to investigate the changes in phase assemblage of powdered cement pastes subjected to a wide range of sulfuric and acetic acid concentrations. A modeling approach utilizing IPHREEQC implemented through Matlab is presented, and the obtained results are compared with pH measurements and compositions of equilibrated calcium and sulfate solutions. The influence of incorporating 11% silica fume (SF) as a replacement for cement predicted a 70% reduction of Portlandite content in the hardened cement paste. Consequently, the acid attack processes and subsequent pH reduction are affected. The modeling approach demonstrates good agreement with experimental data for acetic acid, across a broad range of acid concentrations, for both Portland cement and a blend with SF, without the need for any fitting parameters. However, significant discrepancies between the model and experiments are observed in the case of sulfuric acid. This discrepancy arises due to the formation of lump pieces of material in the experimental setup at higher acid concentrations. These lumps consist of a thin layer of altered hardened cement paste, primarily composed of sulfate-rich phases, encapsulating unaltered hardened cement paste. Since the reaction was not homogeneous and the powder did not entirely react, the sulfuric attack experimental setup was not representative for validating the thermodynamic model.

Keywords

cementitious materials; sulfuric acid attack; silica fume; pozzolanic reaction; thermodynamic modeling; IPHREEQC; solid-liquid phase equilibration experiments

1 Introduction

Portland Cement has limited resistance to aggressive acidic environments, commonly observed in waste-water structures [1–3], containers for animal manure and silage in agricultural applications [4–6], food industry [7], cooling towers, downhole oil-well applications, structures for alternative energy production from biogas or geothermal water, as well as due to natural acid rains and carbonation. Acid attack poses a significant treat to concrete structures, resulting in material loss, decreased section integrity and compromised strength. The long-term performance of cementitious materials is strongly depending on the resistance it can build up against the ingress of aggressive species throughout its porous microstructure with time. Therefore, detailed changes of the phase assemblage composition and experimentally determined information is required about the chemical reactions of aggressive species with the different hydrated phases of the cement paste. These chemical reaction thermodynamic data feed reactive-transport models to predict the long-term deterioration of concrete under various types of acid exposure and different boundary conditions.

All cement phases are thermodynamically unstable at pH values lower than 10 [3; 7–9]. During acid attack the pH of the pore solution decreases, disturbing the equilibrium in the cement paste matrix, and the cement hydration products are dissolved or altered (decalcified) by hydrolytic decomposition, which leads to a severe degradation of the materials properties. As this degradation process proceeds, the thickness of the affected layer and hence its protective performance increases, shifting the dissolution reaction to a diffusion controlled one [5; 9]. Effective diffusivity of the acid species are typically an order of magnitude higher in comparison with the undamaged material [10; 11]. Nitric and acetic acid attack is a typical rapid acidic mechanism resulting in a highly porous degraded layer due to leaching of the formed highly soluble calcium salts (nitrates and acetates) [4–10]. On the other hand,

the slower degradation rates by acids that form low solubility acid-salts, e.g. sulfuric acid, are due to precipitation of a protective layer (e.g. gypsum) that blocks the pores [1–3; 5].

The degradation process of mortar and concrete may be described by different zones which move into the undamaged material with progress of time. These are:

- A zone of erosion, in which the bigger insoluble aggregates are left protruding outwards. The solubility and the grain shape of aggregates have a great influence on the depth of degradation [10; 12].
- A porous degraded layer of low mechanical strength containing silica gel having a pH of the pore solution close to the external acid. This layer also contains Brownmillerite (at pH 3 to 4), aluminum hydroxide gel (pH 3 to 4) and amorphous ferric hydroxide (pH 1 to 2), with the calcium salt of the acid depending on its solubility and the saturation of the liquid [4; 12].
- A transition zone, being a mechanically sound region, where the pH is continuously increasing until reaching the value of the undamaged core material. With a pH drop of the pore solution, portlandite dissolves first followed by calcium silicate hydrate (C-S-H), aluminate ferrite monosulfate (AFm) and aluminate ferrite trisulfate (AFt) [4–8].

The depth of the zones depends on the composition of the material and the type of acid, the concentration and the saturation of the solution they are exposed to. Thermodynamic modeling [3; 4; 7; 8] of acidification and leaching of a CaO-SiO2-H2O system was done in PHREEQC implementing CSH3T solubility model [9; 13] constructed from three C-S-H end members (Figure 1). The leaching and acidification cycle consisted of repeatedly replacing the water solution with 1 kg of aggressive solution and re-equilibrating the hydrated solids. Compared to pure water leaching [9], a much lower number of acidic solution replacements was needed to dissolve the hydrated solids. Acid attack on cementitious materials affects equilibrium concentrations of ions in the cement paste matrix, in accordance with Le Chatelier's principle. Moreover, using thermodynamic modeling, the effect of acid type can be simulated, showing that acetic acid does not precipitate salts ($Ca(acetate)_2$), whereas in case of leaching with sulfuric acid above a concentration of 13 mmol/L, Gypsum starts to precipitate, whose amount significantly increases with acid concentration.

Taheri et al. [14] found an iron-rich layer during sulfuric acid corrosion of steel-reinforcement-free concrete, indicating advanced corrosion depth. Microindentation showed no impact on hardness due to iron enrichment, while softer regions were observed between the iron ring and exposed surface. The group also used µ-XRF for elemental mapping of calcium and sulfur to assess corroded layer thickness [15]. Witkoska-Dobrev et al. [16] studied the effect of acetic acid on the compressive strength of concrete and added various coloring pH indicators to the fresh concrete to determine later after acid attack the penetration depth. Zhao et al. [17] found that for Ordinary Portland Concrete (PC), alkali-activated fly ash and alkali-activated slag mortar acetic acid attack leads to a more enhanced deterioration than for a sulfuric acid attack. Furthermore, according to them, the difference between acetic and sulfuric acid attacks increased with increasing calcium content of the binder. They attribute this to the formation of Gypsum in the corrosion layer, which could act as a barrier against further ingress of sulfuric acid [2]. Dyer [18] studied the resistance of hardened cement paste with and without fly ash for two types of organic acids (acetic and butyric acids) by experiments and thermodynamic modelling. He found that in general both pastes behaved similar but the paste with fly ash had a higher acid resistance due to a lower Portlandite content caused by the pozzolanic reaction. He employed an inverse modelling approach to (empirically) estimate the apparent diffusion coefficient based on the measured pH increase of the exposure (external) solution. In summary, first the thermodynamic description needs to be well understood, adopting equilibration of powdered cements in acidic solutions of varying concentrations [8], which represent fundamental inputs to tackle the transport and kinetics effects in the bulk samples

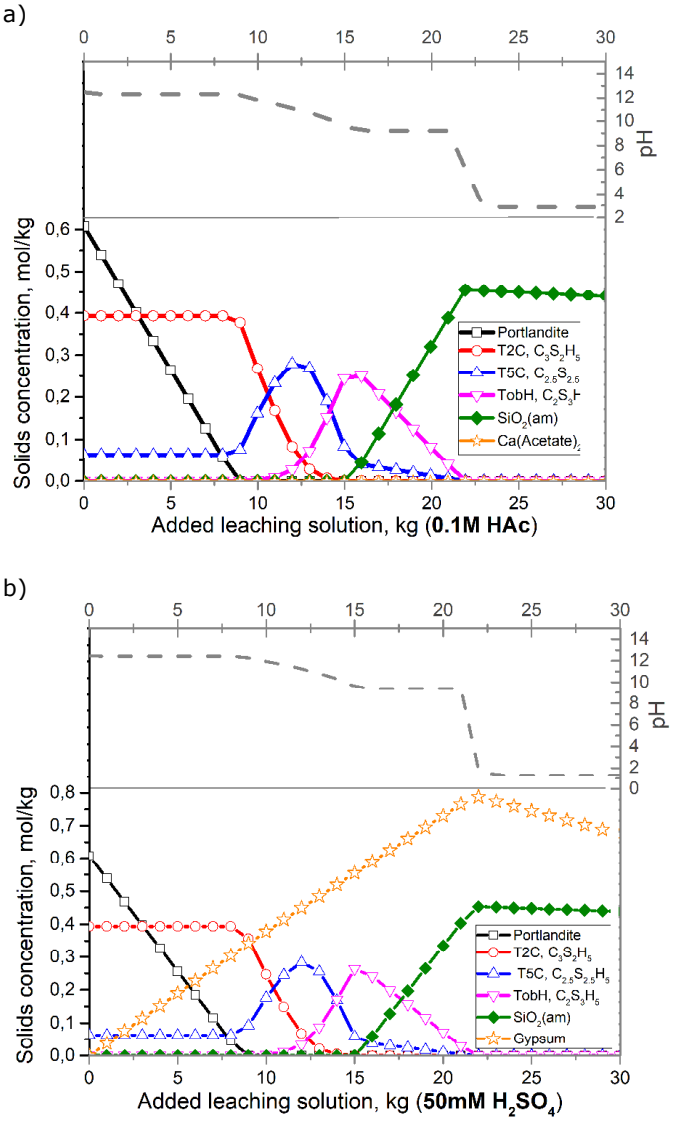

Figure 1 Thermodynamic modeling of portlandite/CSH acidification exposed to a) acetic acid, b) sulphuric acid (adapted from Ukrainczyk et al. [9]).

2 Methodology

2.1 Materials

Chemical and mineralogical compositions of the used cement (CEM I 42.5 R) and silica fume (Elkem 940E), as well as the preparation of hardened cement pastes, without (PC) or with 11% silica fume (PC+SF) are provided in our previous study [8].

2.2 Batch experiments for systematic acidification of cement paste powders

In the experiment, 12.5 g of hardened cement paste, without (PC) or with 11% silica fume (PC+SF), was mixed with systematically varied concentrations of acid. The samples were shaken in closed bottles at room temperature for at least 14 weeks, to stabilize pH. After stabilizations, the suspensions were filtered using 60 mL of deionized water for washing. The original solution and washing water were combined for chemical analysis, and the mass was determined. The metal ion concentrations in the filtered solutions were determined using microwave plasma atomic emission spectrometry. Powder X-ray diffraction was performed using a D8 Advance instrument using Cu-Kα radiation in the 2θ range of 5 to 70°.

2.3 Thermodynamic modeling

A Matlab code detailed in [8] was used to model the acidification and leaching of cement suspensions. The code utilized IPHREEQC and a TD database for cement hydration. The modeling process closely replicated the batch experimental setups by adjusting the solution-to-solids ratios for thermodynamic calculations. The model consisted of two sections: first, the input parameters for cement composition and water/cement ratio were used for hydration calculations, and second, the resulting solid composition was exposed to solutions of water and various concentrations of acids. The equilibrium results from the model were compared to the batch reaction experiments for better estimation of the effects of different acids, their concentrations, and variations in hydrated paste compositions. Solid phase volumes are obtained from phase concentrations in remaining solids and their molar volumes, while fractions are related to the volume of the initial bulk paste calculated from the w/c ratio and their unhydrated densities.

3 Results and discussion

After pH stabilization of the suspensions in sulfuric acid (H_2SO_4), the samples displayed varying colors in both the liquid and solid fractions, as depicted in Figure 2. For the liquid fraction of PC, three distinct colorations were observed: colorless and light red/brown (around pH 10-9.5). The color of PC solids transitioned from light grey to dark red/brown (peaking at around pH 10-9.5) and back to light brown and finally whiteish. In the case of PC+SF, the liquid phase appeared semi-transparent, while the solids exhibited transitions in colorations from light grey to brown grey and light grey whiteish. The reddening of the liquid and solid phases at medium pH values is due to dissolution or concentration of iron compounds, while at lower pH values the coloration is becoming grey and whiteish due to precipitation of sulfate salts. For comparison, the acetic acid results (shown in [8]) show intense reddening of the liquid phases for low pH values due to leached iron forming red ferric acetate aqueous complex and reddish brown ferric hydroxide colloid.

Already in the case of acetic acid [8] several experimental challenges were identified. The most significant concerned the washing of the solid fraction during filtration. It was found, that washing on the one hand prevented the enrichment of the solid phase with subsequently precipitated phases while on the other hand probably influenced the stability and therefore the inventory of the phases. In the case of H_2SO_4, an additional challenge was identified: in experiments with powder samples at higher H_2SO_4 acid concentrations lump pieces of material were formed, which consisted of a thin yellow-brownish layer of altered

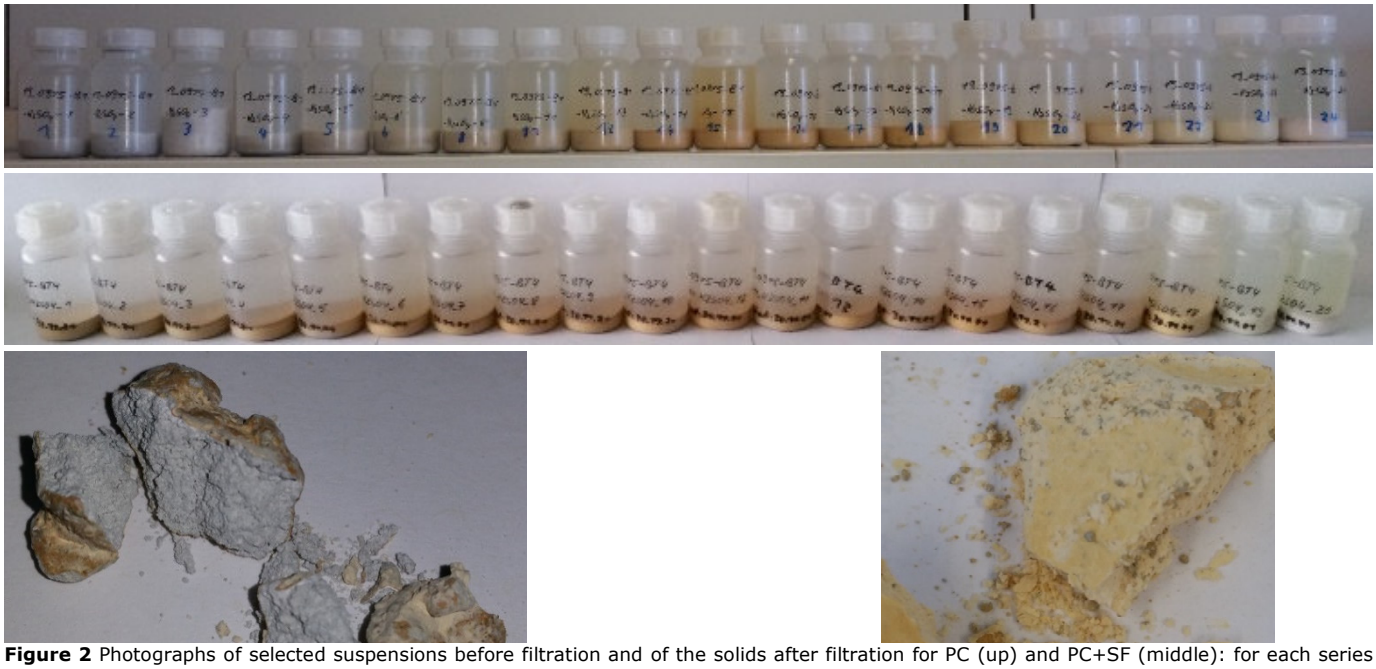

Figure 2 Photographs of selected suspensions before filtration and of the solids after filtration for PC (up) and PC+SF (middle): for each series with decreasing pH from left to right. Some of the solid fractions after filtration for PC with 6.36 mM H_2SO_4 per g_{hcp} (down, left) and PC+SF with 2.932 mM H_2SO_4 per g_{hcp} (down, right)

hardened cement paste (mostly sulfate-rich phases, with encapsulated grey unaltered hardened cement paste inside (Figure 2). In Figure ***3***, the mineralogical phases for the powder (main fraction after filtration) and the lump pieces are shown exemplarily for one acid concentration. The powder shows distinct peaks with high intensity due to the large share of crystalline parts. In this case, it consists mainly of Gypsum. By contrast, the lump pieces contain a far less fraction of crystalline parts due to the encapsulated unaltered cement paste. Only Gypsum and Ettringite as part of the capsule layer can be detected.

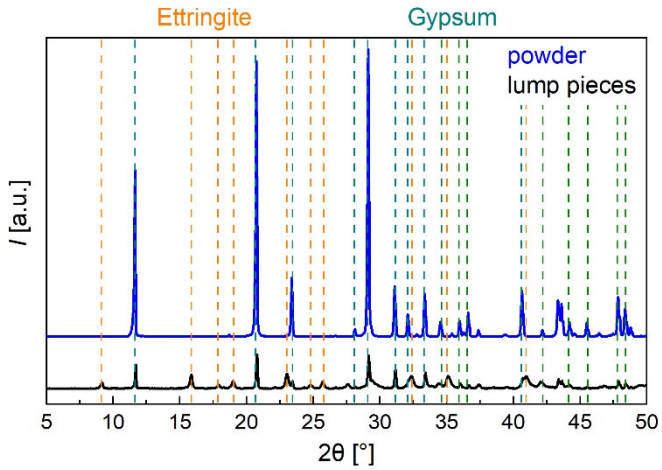

Figure 3 XRD diffraction patterns of the two solid fractions after filtration for PC with 6.4 mM H_2SO_4 per g_{hcp}: the few lump pieces and the powder (vertically shifted).

These experimental artifacts thus explain the large discrepancies observed between the model and experiments in the case of sulfuric acid (H_2SO_4), as can be seen in Figure 4. The deviation is increasing with the sulfuric acid dosage more strongly for the blended cement (PC+SF) than for the reference PC. This can be attributed to the less Portlandite (lower pH buffering) and the denser (C-S-H) microstructure, that hinders the dissolution more effectively even at lower acid dosages. At higher H_2SO_4 acid concentrations lump pieces of material were formed, kinetically limiting the dissolution reactions, thus not representative for thermodynamic equilibrium conditions. Since not all powder reacted and no homogeneous composition resulted, the experiments where not representative for validating the model. At low acid concentrations, below a few millimoles of sulfuric acid per gram of hydrated cement paste (hcp), the pH remains relatively constant, with a value above 12, in both PC and PC+SF. This is primarily due to the buffering effect provided by Portlandite. As the acid concentration increases, the pH gradually decreases, transitioning from gradual to more abrupt changes. The drop in pH begins at higher acid concentrations for PC compared to PC+SF, indicating a stronger buffering effect due to a higher Portlandite content. The modeled curves exhibits a drop in pH values from 12 to 10 attributed to the buffering effect resulting from the incongruent dissolution, primarily decalcification, of the C-S-H solid solution with a variable Ca/Si ratio (as shown in Figure 6). The model curve exhibits two additional plateaus, at values around ten and nine. These plateaus are attributed to the buffering effect resulting from the dissolution of ettringite, C3AFSH solid solution and Thaumasite, respectively (as shown in Figure 6). The amount of measured dissolved calcium ion is slightly decreasing with acid dosage. This is contrary to the model predictions, which show strong increase after a threshold acid dosage of 4 mM/g_{hcp}.

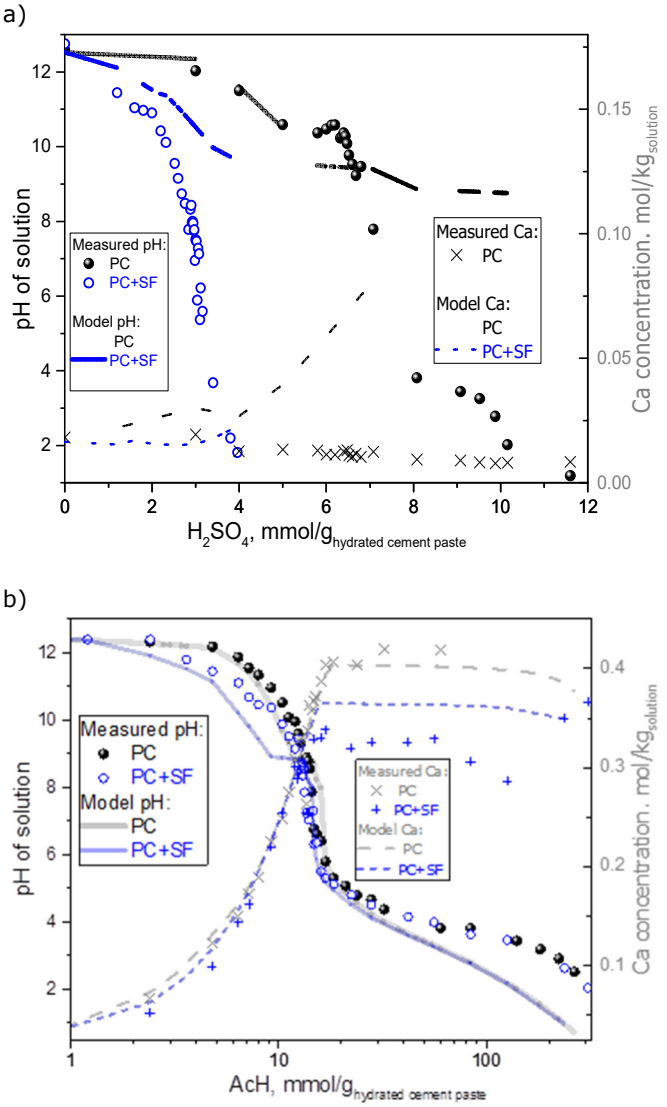

Figure 4 Model validation on batch equilibration tests, for both PC and PC+SF hydrated cement paste powders. Change of pH and dissolved calcium as a function of acid concentration for H_2SO_4 (a) and acetic acid AcH (b). The discrepancies in the case of H_2SO_4 can be explained with experimental artifacts.

In contrast to H_2SO_4, for acetic acid (AcH), the applied modelling approach showed an overall good agreement with experiments over a very broad range of acid concentrations [8], both for PC and PC+SF (Figure 4b), resulting in a relative root square mean error of below 10% for pH and calcium (in solution and remaining solids), without applying any fitting parameter. This agreement is remarkable considering a particular challenge proved to be the development of a filtration and washing process. On the one hand, washing was suitable for removing the acetates and acetate hydrates precipitated during filtration but, on the other hand, prevented or minimized the alteration of the phase inventory by changing the ion concentrations and the pH value and thus the stability of some phases during washing.

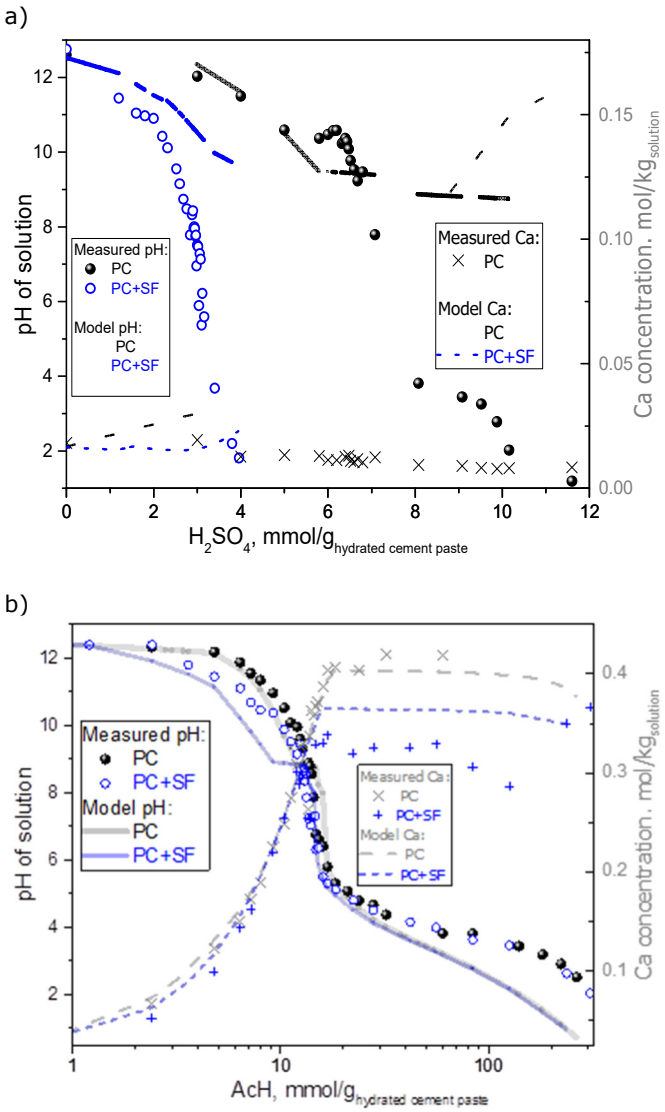

Figure 4 Model validation on batch equilibration tests, for both PC and PC+SF hydrated cement paste powders. Change of pH and dissolved calcium as a function of acid concentration for H2SO4 (a) and acetic acid AcH (b). The discrepancies in the case of H2SO4 can be explained with experimental artifacts.

The main discussion that could be drawn from this comparison of modelling and experiments (Figure 4) are as follows. The change in mineral composition (see Figure ***6***) due to SF addition (PC+SF) leads to an earlier decrease of pH due to less buffering effect of Portlandite and lower overall Ca content. The discrepancies increased with acid dosage, and for very high acetic acid dosages after depletion of primary hydrated phases, are related to uncertainties of the model in predicting secondary Al-gel, Si-gel and Fe-gel precipitates. The discrepancy at high acid concentrations (equilibrium pH < 4) could also be explained by challenges in sample preparation, especially the observed artifacts due to drying and/or precipitation (primarily Ca- and Al-acetate salts) during the filtration of the remaining solids after acid exposures could be a reason for this.

The model predicted the mineralogical composition of the remaining solid phases, as depicted in Figure 6. The volume fractions of these phases were determined relative to the initial volume of the hydrated cement paste, enabling quantification of changes in total porosity resulting from sulfate precipitation and dissolution reactions as acid concentration increased. Notably, the porosity decreased due to the precipitation of ettringite and gypsum minerals, expanding the cement paste volume by a factor of 1.25 (1.20 for PC+SF). After reaching a critical dosage of H_2SO_4 at 5 mM/g, Ettringite (and Thaumasite at 10 mM/g) dissolution was initiated, rapidly reducing the total volume of the paste.

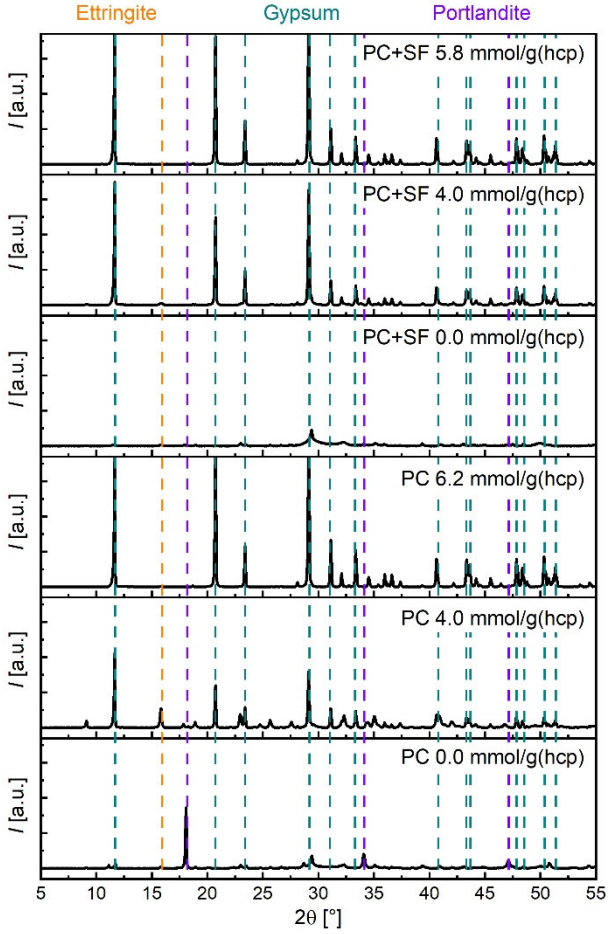

Figure 5 XRD diffraction patterns for low concentrations of H_2SO_4 for PC and PC+SF.

XRD analysis (Figure 5) for PC showed even for samples treated with 4.0 mM H2SO4 per gram of hydrated cement paste no detectable Portlandite diffraction peaks, which are clearly visible without any acid. For PC+SF, no portlandite peaks at all could be detected. Probably, the sample without treatment with acid was not dry enough since it would be expected, that PC+SF shows a higher amount of Portlandite. For the samples after treatment with acid, only small differences between PC and PC+SF can be detected. The samples with silica fume exhibit overall more crystalline fractions, more Gypsum and less Ettringite. However, due to the described experimental challenges, the interpretation of this data should be done with caution. Notably, the mixture without silica fume exhibited a higher fraction of Portlandite. The addition of SF (11% replacement of cement) resulted in a reduction of Portlandite content from 22% to 6.7% [8], assuming a nearly complete pozzolanic reaction in the model. Consequently, higher concentrations of C-S-H phases were observed (see Figure 6). The higher content of Portlandite in PC samples, along with its pH buffering effect at low acid concentrations, led

to the initiation of C-S-H phase decalcification and dissolution of other phases at higher acid concentrations compared to PC+SF samples.

a)

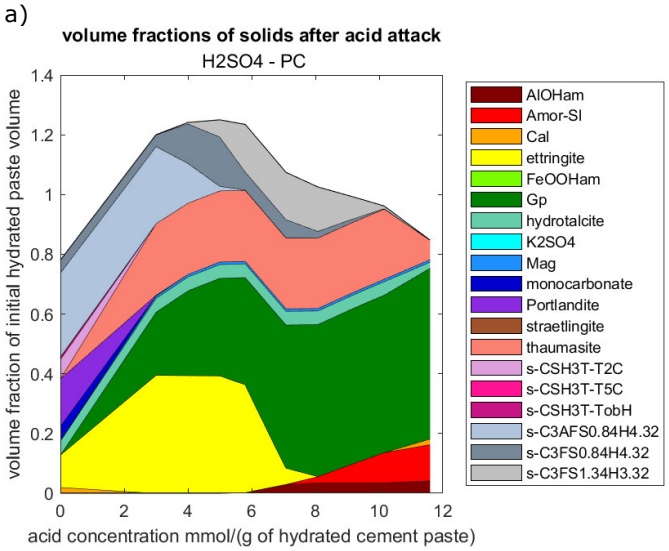

b)

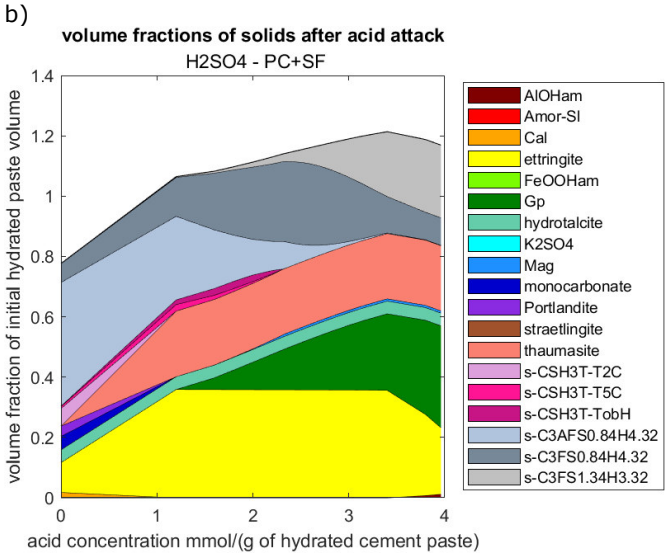

Figure 6 Predicted volume fractions and porosity as a function of sulfuric acid concentration in PC (a) and PC+SF (b). Phase volumes are obtained from phase concentrations in remaining solids and their molar volumes, while fractions are related to the volume of the initial bulk paste calculated from the w/c ratio and their unhydrated densities.

The lower content of C-S-H, Ettringite and Thaumasite phases in PC+SF samples resulted in reduced volume expansion and a narrower range of acid concentrations at which dissolution occurred. The critical H_2SO_4 dosage was shifted from 5 mM/g to 3.5 mM/g due to the presence of SF, leading to earlier dissolution of Ettringite and Thaumasite. At the final acid dosage, both mixtures predominantly consisted of Gypsum and amorphous silica (SiO2) in the remaining solids, with the model not capturing their water content.

Figure 7 shows the measured amount of dissolved aqueous species in the solution. Measured dissolved calcium ion has a decreases overall trend with acid dosage, contrary to model predictions which show a strong increase after a threshold acid dosage of 4 mM/g_{hcp} (Figure 4). Amount of dissolved silicium slightly increases after around 5 mM/g acid dosage and ends with a final significant increase after around 10 mM/g dosage, due to dissolution of C3AFSH solid solution. This increase in silicium after 10 mM/g dosage, is accompanied by simultaneous increase in aluminium and magnesium species in solution. The iron species do not show such a drastic increase in solution.

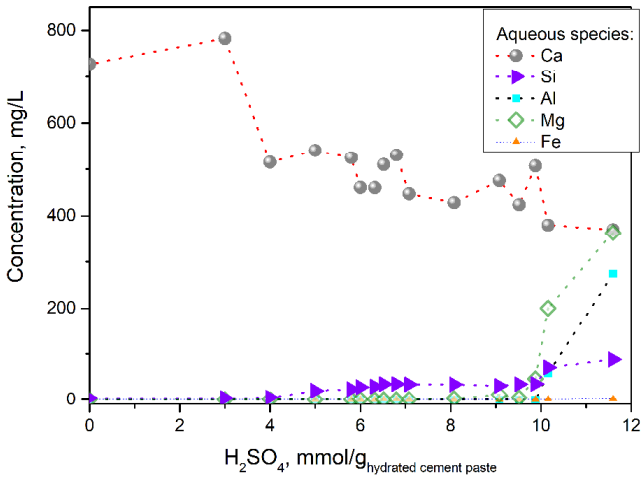

Figure 7 Concentration of dissolved (Ca, Si, Al, Mg and Fe) elements as a function of acid concentration for PC sample.

Measured values for a dissolved sulphate in the PC system show significant increase after H2SO4 acid dosage of 5 mM/g (Figure 8). This agrees with the thermodynamic modeling (Figure 4) predicting the dissolution of the ettringite phase. Figure 8 also depicts the amount of precipitated sulfates, calculated as a difference between the added and dissolved amount. It can be observed that until that threshold value (5 mM/g) there is a linear relationship of the precipitated sulfate as a function of added sulfuric acid. After this threshold, the precipitation approaches a stable value, resulting in a significant increase of sulfates concentration dissolved in the solution.

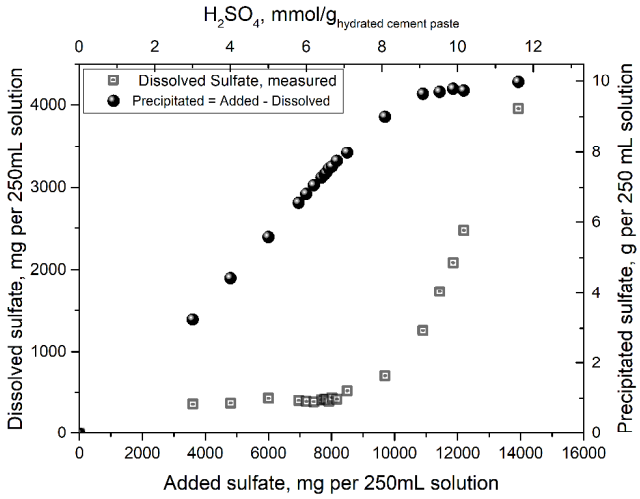

Figure 8 Dissolved and precipitated sulphate in the PC system.

4 Conclusion

From the results of this study, the following conclusions can be drawn.

1. Thermodynamic modeling suggests that incorporating 11% silica fume (SF) as a cement replacement reduces

the Portlandite content from 22% to 6.7% while increasing the amount of C-S-H phase. The model assumes complete pozzolanic reaction.
2. The inclusion of SF in the initial mineral composition causes an earlier decrease in pH due to reduced buffering effect of Portlandite and lower overall calcium content.
3. Batch experiments with sulfuric acid revealed unexpected lump formation, deviating significantly from model predictions. These lumps impeded complete degradation reactions, introduced non-homogeneity, and posed challenges for model validation.
4. The use of acetic acid eliminates the precipitation of acid salts. The modeling approach applied demonstrates good agreement (below 10% error) with experimental results for pH and dissolved calcium, without employing any fitting parameters.
5. Employing H_2SO_4 results in decreased porosity of cement paste due to the precipitation of Ettringite, Gypsum, and Thaumasite minerals. This expansion of the cement paste volume by a factor of 1.25 (PC) or 1.20 (PC+SF) occurs until a critical H_2SO_4 dosage of 5 mM/g (PC) or 3.5 mM/g (PC+SF) is reached. After reaching this threshold dosage, dissolution of Ettringite (and Thaumasite at 10 mM/g) commences, rapidly reducing the theoretical volume of the paste. This observation aligns with the measured increase in dissolved sulfate in the PC system beyond the threshold dosage.
6. A linear relationship between the measured precipitated sulfate and the added sulfuric acid was observed until the threshold value of 5 mM/g for PC was reached.

Acknowledgement

This research was funded by the German Research Foundation (DFG) under the joint project number 426807554, titled "Experimentally supported multi-scale Reactive Transport modelling of cementitious materials under Acid attack (ExpeRTa)" involving the two research institutes under grant numbers KO 3203/5-1 and DE 821/12-1. The authors would like to thank HeidelbergCement AG for providing the cement and Elkem ASA Silica Materials for providing the silica fume.

References

[1] Grengg, C. et al. (2018) *Advances in concrete materials for sewer systems affected by microbial induced concrete corrosion: A review* in: Water Research 134, pp. 341–352. https://doi.org/10.1016/j.watres.2018.01.043

[2] Grengg, C. et al. (2020) *Long-term in situ performance of geopolymer, calcium aluminate and Portland cement-based materials exposed to microbially induced acid corrosion* in: Cement and Concrete Research 131, p. 106034. https://doi.org/10.1016/j.cemconres.2020.106034

[3] Yuan, H. et al. (2015) *Degradation modeling of concrete submitted to biogenic acid attack* in: Cement and Concrete Research 70, pp. 29–38. https://doi.org/10.1016/j.cemconres.2015.01.002

[4] Bertron, A.; Duchesne, J.; Escadeillas, G. (2005) *Attack of cement pastes exposed to organic acids in manure* in: Cement and Concrete Composites 27, 9-10, pp. 898–909. https://doi.org/10.1016/j.cemconcomp.2005.06.003

[5] Koenig, A.; Dehn, F. (2016) *Main considerations for the determination and evaluation of the acid resistance of cementitious materials* in: Materials and Structures 49, Nr. 5, pp. 1693–1703. https://doi.org/10.1617/s11527-015-0605-7

[6] Ukrainczyk, N. et al. (2019) *Geopolymer, Calcium Aluminate, and Portland Cement-Based Mortars: Comparing Degradation Using Acetic Acid* in: Materials 12, Nr. 19, p. 3115. https://doi.org/10.3390/ma12193115

[7] Windt, L. de et al. (2015) *Interactions between hydrated cement paste and organic acids: Thermodynamic data and speciation modeling* in: Cement and Concrete Research 69, pp. 25–36. https://doi.org/10.1016/j.cemconres.2014.12.001

[8] Berger, F. et al. (2022) *Thermodynamic Modeling and Experimental Validation of Acetic Acid Attack on Hardened Cement Paste: Effect of Silica Fume* in: Materials 15, Nr. 23, p. 8355. https://doi.org/10.3390/ma15238355

[9] Ukrainczyk, N.; Walker, C.; Koenders, E. (2018) *Numerical modelling of cementitious materials ageing under acid attack* in:

[10] Beddoe, R. E.; Dorner, H. W. (2005) *Modelling acid attack on concrete: Part I. The essential mechanisms* in: Cement and Concrete Research 35, Nr. 12, pp. 2333–2339. https://doi.org/10.1016/j.cemconres.2005.04.002

[11] Perko, J. et al. (2020) *Influence of Micro-Pore Connectivity and Micro-Fractures on Calcium Leaching of Cement Pastes—A Coupled Simulation Approach* in: Materials 13, Nr. 12, p. 2697. https://doi.org/10.3390/ma13122697

[12] Koenig, A.; Dehn, F. (2016) *Biogenic acid attack on concretes in biogas plants* in: Biosystems Engineering 147, pp. 226–237. https://doi.org/10.1016/j.biosystemseng.2016.03.007

[13] Walker, C. S. et al. (2016) *Calcium silicate hydrate (C-S-H) gel solubility data and a discrete solid phase model at 25 °C based on two binary non-ideal solid solutions* in: Cement and Concrete Research 79, pp. 1–30. https://doi.org/10.1016/j.cemconres.2015.07.006

[14] Taheri, S. et al. (2021) *Migration and formation of an iron rich layer during acidic corrosion of concrete with no steel reinforcement* in: Construction and Building Materials 309, p. 125105. https://doi.org/10.1016/j.conbuildmat.2021.125105

[15] Taheri, S. et al. (2020) *Corrosion Inhibitory Effects of Mullite in Concrete Exposed to Sulfuric Acid Attack* in: Corrosion and Materials Degradation 1, H. 2, S. 282–295. https://doi.org/10.3390/cmd1020014

[16] Witkowska-Dobrev, J. et al. (2021) *Effect of Acetic Acid on Compressive Strength and Geometric Texture of the Surface of C20/25 Class Concrete* in: Sustainability 13, Nr. 9, p. 5136. https://doi.org/10.3390/su13095136

[17] Zhao, W. et al. (2022) *Characterization and Comparison of Corrosion Layer Microstructure between Cement Mortar and Alkali-Activated Fly Ash/Slag Mortar Exposed to Sulfuric Acid and Acetic Acid* in: Materials 15, Nr. 4, p. 1527. https://doi.org/10.3390/ma15041527

[18] Dyer, T. (2017) *Influence of cement type on resistance to attack from two carboxylic acids* in: Cement and Concrete Composites 83, pp. 20–35. https://doi.org/10.1016/j.cemconcomp.2017.07.004